



FULL LENGTH ARTICLE

# SETDB1-mediated CD147-K71 di-methylation promotes cell apoptosis in non-small cell lung cancer



Ming-Yan Shi <sup>1</sup>, Yarong Wang <sup>1</sup>, Ying Shi <sup>1</sup>, Ruofei Tian, Xiaohong Chen, Hai Zhang, Ke Wang\*, Zhinan Chen\*, Ruo Chen\*

National Translational Science Center for Molecular Medicine & Department of Cell Biology, Fourth Military Medical University, Xi'an, Shaanxi 710032, China

Received 11 November 2022; received in revised form 19 January 2023; accepted 3 February 2023  
Available online 24 March 2023

## KEYWORDS

CD147 di-methylation;  
Cell apoptosis;  
FOSB;  
Non-small cell lung cancer;  
SETDB1

**Abstract** Protein post-translational modifications (PTMs) are at the heart status of cellular signaling events and broadly involved in tumor progression. CD147 is a tumor biomarker with various PTMs, promoting tumor metastasis and metabolism reprogramming. Nevertheless, the relationship between the PTMs of CD147 and apoptosis has not been reported. In our study, we produced a specific anti-CD147-K71 di-methylation (CD147-K71me<sub>2</sub>) antibody by immunizing with a di-methylated peptide and observed that the level of CD147-K71me<sub>2</sub> in non-small cell lung cancer (NSCLC) tissues were lower than that in NSCLC adjacent tissues. SETDB1 was identified as the methyltransferase catalyzing CD147 to generate CD147-K71me<sub>2</sub>. RNA-seq showed that FOSB was the most significant differentially expressed gene (DEG) between wild-type CD147 (CD147-WT) and K71-mutant CD147 (CD147-K71R) groups. Subsequently, we found that CD147-K71me<sub>2</sub> promoted the expression of FOSB by enhancing the phosphorylation of p38, leading to tumor cell apoptosis. *In vivo* experiments showed that CD147-K71me<sub>2</sub> significantly inhibited tumor progression by promoting cell apoptosis. Taken together, our findings indicate the inhibitory role of CD147-K71me<sub>2</sub> in tumor progression from the perspective of post-translational modification, which is distinct from the pro-cancer function of CD147 itself, broadening our perspective on tumor-associated antigen CD147.

© 2023 The Authors. Publishing services by Elsevier B.V. on behalf of KeAi Communications Co., Ltd. This is an open access article under the CC BY-NC-ND license (<http://creativecommons.org/licenses/by-nc-nd/4.0/>).

\* Corresponding author.

E-mail addresses: [wangke@fmmu.edu.cn](mailto:wangke@fmmu.edu.cn) (K. Wang), [znchen@fmmu.edu.cn](mailto:znchen@fmmu.edu.cn) (Z. Chen), [novababe@126.com](mailto:novababe@126.com) (R. Chen).

Peer review under responsibility of Chongqing Medical University.

<sup>1</sup> These authors contributed equally.

## Introduction

Resisting cell death is one of the hallmarks of cancers.<sup>1</sup> As a common form of cell death, cell apoptosis is closely related to tumor progression in addition to some physiological processes including embryonic development and clearance of senescent cells.<sup>2</sup> Tumor cells usually resist cell apoptosis through various routes, such as the disrupted balance between pro-apoptotic and anti-apoptotic proteins, impaired death receptor signaling, and reduced caspase activity.<sup>3–7</sup> Given the importance of apoptosis in tumor progression, the strategies for cancer treatment targeting apoptotic defects have been approved in clinical application. Small molecule inhibitors of anti-apoptotic protein Bcl-2 show safety and efficacy in patients with acute myeloid leukemia, chronic lymphocytic leukemia, and mantle-cell lymphoma.<sup>8–10</sup> Hence, it is necessary to explore the mechanism of tumor cell apoptosis, providing a more theoretical basis for tumor therapy targeting apoptosis routes.

Protein post-translational modifications (PTMs), which include phosphorylation, methylation, ubiquitination, and acetylation,<sup>11</sup> draw more and more attention owing to their crucial roles in tumor proliferation, metastasis, metabolism reprogramming, and immune escape.<sup>12–16</sup> It is reported that methylation, a common PTM in malignant tumors, participates in the regulation of tumor cell apoptosis. Methyltransferase Set9-mediated E2F1-K185 methylation prevents the activation of its proapoptotic target gene and accelerates tumor progression.<sup>17</sup> The methylation of H3K9 catalyzed by methyltransferase SETDB1 facilitates p53-dependent apoptosis by repressing APAK.<sup>18</sup> Tazemetostat, an EZH2 inhibitor, decreases effectively the tri-methylation level of H3K27 and inhibits the progression of pediatric malignant rhabdoid tumors by inducing cell apoptosis.<sup>19</sup>

CD147, also known as extracellular matrix metalloproteinase inducing factor, contributes to tumor progression by various approaches, including resisting cell apoptosis.<sup>20,21</sup> In our previous study, we have identified di-methylations of CD147 at different lysine residues, and the di-methylation of CD147-K234 promotes non-small cell lung cancer (NSCLC) progression by enhancing glycolysis and lactate export of tumor cells.<sup>22</sup> However, the relationship between CD147 di-methylation and tumor cell apoptosis remains unclear.

Our study found low CD147-K71me2 levels in NSCLC tissues compared with adjacent tissues. Methyltransferase SETDB1-mediated CD147-K71me2 facilitates tumor cell apoptosis by enhancing FOSB expression, which inhibits tumor progression. Our study reveals the relationship between CD147 di-methylation and tumor cell apoptosis and provides novel insight for understanding NSCLC pathogenesis from the perspective of PTMs.

## Materials and methods

### Non-small cell lung cancer tissues

NSCLC and their adjacent tissues ( $n = 28$ ) were collected from Tangdu Hospital of Forth Military Medical University.

The clinicopathological parameters of the NSCLC individuals are shown in Table 1.

### Cell culture

The cell lines were obtained from the American Type Culture Collection (A549) and the Cell bank of the Chinese Academy of Sciences (NCI-H460 and HEK293T), which were cultured in an incubator with 5% CO<sub>2</sub> at 37 °C. The culture medium was RPMI 1640 medium containing 10% fetal bovine serum, 2% L-glutamine, and 1% penicillin/streptomycin.

### Construction of stable cell lines

The lentivirus16 for CD147 silencing was previously constructed by our laboratory,<sup>23</sup> which was used to construct CD147 knockdown cell lines (A549/H460-shCD147). The lentiviruses encoding wild-type CD147 and mutant CD147 (CD147-K71R) genes (GENECHEM, China) were transfected into A549/H460-shCD147 cell lines to generate wild-type CD147 (A549/H460-rCD147-WT) and mutant CD147 (A549/H460-rCD147-K71R) cell lines, respectively. All the stable cell lines were screened with 5 µg/mL puromycin after 48-h transfection.

### Plasmids

The plasmid pcDNA3.1-CD147 was constructed by inserting CD147 gene into pcDNA3.1 vector.<sup>24</sup> The pcDNA3.1-CD147-K71R plasmid was generated from the pcDNA3.1-CD147 plasmid by a Fast Site-Directed Mutagenesis Kit (KM101,

**Table 1** The clinicopathological parameters of individuals with NSCLC.

Parameters	N
<b>Gender</b>	
Male	21
Female	7
<b>Pathological subtype</b>	
Lung adenocarcinoma	12
Lung squamous cell carcinoma	11
Adenosquamous carcinoma	5
<b>T staging</b>	
T1+T2	15
T3+T4	13
<b>N staging</b>	
N0	13
N1+N2+N3	15
<b>M staging</b>	
M0	28
M1	0
<b>AJCC staging</b>	
I+II	14
III+IV	14
<b>Total</b>	<b>28</b>

TIANGEN). The plasmid SETDB1 was constructed by cloning SETDB1 gene (NM\_001145415.1) into pcDNA3.1 (+)-C-DYK vector (GenScript, China).

### Gene overexpression and silence

The cells were transfected with siRNA or plasmids using a jetPRIME transfection kit (PT-114-15, Polyplus, France) according to the manufacturer's instructions. The sequences for siRNA are listed in [Table S1](#).

### Western blot and dot blot

The cells and NSCLC tissues were lysed with RIPA lysis buffer (P0013B, Beyotime, China) containing phenylmethanesulfonyl fluoride (ST505, Beyotime, China) and phosphatase inhibitor (4693159001, Roche, Switzerland) and protein quantitation was conducted with the BCA protein assay kit (23227, Thermo Scientific, USA). The protein samples were subjected to different concentrations of SDS-PAGE gel electrophoresis and then transferred onto PVDF membranes (IPVH00010, Millipore, USA). After being blocked with 5% bovine serum albumin for 1 h at room temperature, the membranes were incubated at 4 °C overnight with the corresponding primary antibodies. The images were obtained with a Gel Doc EZ Imager (BIO-RAD) after incubation with secondary HRP-labeled antibodies for 1 h at room temperature. The data were analyzed by Image Lab software (BIO-RAD). The NC membranes were used to perform the dot blot assay. The peptides ([Table S2](#)) used in dot blot were synthesized by ChinaPeptides (Shanghai, China) and CHINESE PEPTIDE (Hangzhou, China). The antibodies used in Western blot are listed as follows: anti-CD147 (HAb18; produced in our laboratory; dilution 1:3000), anti-CD147-K71me2 (ABclonal; dilution 1:2000), anti-Tubulin (Proteintech; dilution 1:5000), anti- $\beta$  actin (HUABio; dilution 1:5000), anti-SETDB1 (Proteintech; dilution 1:2000), anti-FOSB (CST; dilution 1:2000), anti-JNK (CST; dilution 1:1000), anti-p-JNK (CST; dilution 1:1000), anti-P38 (HUABio; dilution 1:2000), anti-p-p38 (HUABio; dilution 1:2000), anti-ERK1/2 (HUABio; dilution 1:2000), anti-p-ERK1/2 (CST; dilution 1:2000), anti-Caspase3 (Proteintech; dilution 1:2000), anti-Bax (Proteintech; dilution 1:10,000), anti-Bcl2 (Proteintech; dilution 1:5000), HRP-Goat anti-mouse IgG (H+L) secondary antibody (Thermo Fisher Scientific (31430); dilution 1:5000), HRP-Goat anti-rabbit IgG (H+L) secondary antibody (Thermo Fisher Scientific (31460); dilution 1:5000). In dot blot assay, the dilution ratios for anti-CD147-K71me2 antibody were 1:200, 1:400, 1:800, 1:1600, 1:3200, 1:6400, 1:12,800, 1:25,600, and 1:51,200.

### Real-time quantitative PCR

Total RNA was extracted with Total RNA Kit II (D6934-01, OMEGA-BIO-TEK, USA) and transcribed into cDNA with PrimeScript™ RT Master Mix Kit (RR036A, Takara, Japan) according to the manufacturers' instructions. Real-time quantitative PCR was performed with TB Green® Premix Ex Taq™ II (RR820A, TaKaRa, Japan), and the actin gene was

used as a control. The sequences for primers are shown in [Table S3](#).

### *In vitro* methyltransferase assay

The K71 peptide (1  $\mu$ g) was incubated with 1  $\mu$ g of SETDB1 expressed and purified from HEK293T cells in methyltransferase buffer (50 mM Tris-HCl pH 8.5, 100 mM NaCl, 10 mM DTT, 1 mM PMSF, 20 mM SAM) for 2–3 h at 37 °C. The dot blot assay was conducted to detect CD147-K71me2.

### Co-immunoprecipitation (Co-IP)

The Co-IP assays were performed using the Pierce Co-Immunoprecipitation Kit (26149, Thermo Fisher Scientific, USA) according to the manufacturer's protocol. Anti-CD147 (HAb18) antibody was used for antibody immobilization. The eluted samples obtained from the Co-IP assay were analyzed by Western blot.

### Immunoprecipitation (IP)

IP assay was performed using the Pierce Crosslink Immunoprecipitation Kit (26147, Thermo Fisher Scientific, USA) according to the manufacturer's protocol. Anti-CD147 (HAb18) antibody was used for antibody immobilization. The eluted samples obtained from the IP assays were identified by Coomassie blue staining and analyzed by Western blot.

### Specific peptide-blocking assay

Saturated CD147-K71me2 peptide was mixed with anti-CD147-K71me2 antibody at room temperature for 30 min. The CD147-K71me2 peptide samples and protein samples lysed from A549 and H460 cells were detected using the mentioned mixture of CD147-K71me2 peptide and anti-CD147-K71me2 antibody by dot blot and Western blot to evaluate the specificity of anti-CD147-K71me2 antibody.

### Immunofluorescence staining

For cellular immunofluorescence staining, A549 and H460 cells were seeded onto glass dishes overnight, fixed with 4% paraformaldehyde (AR1069, Boster, USA), and permeabilized with 0.02% Triton X-100 (A600198-0500, BBI Life Sciences). After being blocked with 10% goat serum, the cells were incubated with anti-CD147 (HAb18) (dilution 1:100) and anti-SETDB1 (11231-1-AP; Proteintech; dilution 1:100) antibodies overnight at 4 °C and the corresponding fluorescently labeled secondary antibodies (Alexa Fluor555-labeled, highly cross-adsorbed donkey anti-rabbit IgG (H+L) from Thermo Fisher Scientific; A-31572; dilution 1:200; Alexa Fluor488-labeled, highly cross-adsorbed donkey anti-mouse IgG (H+L) from Thermo Fisher Scientific; A-21202; dilution 1:200) for 1 h at room temperature sequentially. A confocal fluorescence microscope (Nikon) was used to evaluate the co-localization of CD147 and SETDB1. For NSCLC tissue immunofluorescence staining, paraffin sections were dewaxed, followed by antigen

retrieval in citrate repairing buffer (10  $\mu\text{mol/L}$ , pH 6.0). The subsequent steps were consistent with the method used for cellular immunofluorescence staining.

### Cell counting kit-8 (CCK-8) assay

Cell proliferation was analyzed using a CCK-8 kit (C0005, Topscience, USA). The cells (2000 cells per well) were seeded into 96-well plates and detected with CCK-8 reagent at 0 h, 24 h, 48 h, 72 h, and 96 h using a microplate reader (optical density = 450 nm).

### Flow cytometric analysis of cell apoptosis

The percentage of apoptotic cells was detected by the commercial kits (APC Annexin V Apoptosis Detection Kit with PI, 640932; FITC Annexin V Apoptosis Detection Kit with PI, 640914, Biolegend, USA). The corresponding cells were stimulated by cisplatin (4  $\mu\text{g/mL}$ ) for 48 h and collected for flow cytometry according to the manufacturer's protocols. The percentage of apoptotic cells was analyzed using a FACSCalibur flow cytometer (BD Biosciences, USA).

### *In vivo* experiments

The animal study was approved by the Institutional Animal Care and Use Committee of the National Translational Science Center for Molecular Medicine. BALB/c nude mice (6 weeks, female) purchased from Beijing Vital River Laboratory Animal Technologies were randomized into two groups ( $n = 8$  per group) and subcutaneously injected with A549-rCD147-WT and A549-rCD147-K234R cells ( $2 \times 10^7$  cells/mL in 0.1 mL medium), respectively. After 3–4 weeks, the tumor masses were removed from the mouse body to measure the tumor weight and volume. The tumor tissues were used to make tissue sections for TUNEL assay and immunohistochemistry staining. The rest of the tissues were used to perform Western blot assays.

### TUNEL assay

Paraffin sections from mouse tumor tissue were used for the TUNEL assays. The Apoptosis Assay Kit (ab206386, Abcam, UK) was used to evaluate the apoptosis of tumor tissues according to the manufacturer's instructions. The data were collected using a Nikon microscope. For each tissue, three random fields were selected and evaluated by ImageJ.

### Immunohistochemistry analysis

Paraffin sections from mouse tumor tissue were used for immunohistochemistry analysis. Paraffin sections were dewaxed, followed by antigen retrieval in citrate repairing buffer (10  $\mu\text{mol/L}$ , pH 6.0). After being soaked in methanol containing 3% hydrogen peroxide for 10 min, the sections were washed with PBS for 15 min, blocked using 10% goat serum for 20 min, and incubated with anti-Ki-67 (ab16667; Abcam, UK; dilution 1:200) and anti-Bcl2 (12789-1-AP;

Proteintech, China; dilution 1:200) antibodies overnight at 4 °C. Immunoperoxidase staining was conducted using a General SP kit (SP-9000, ZSGB-BIO, China), and the sections were treated with 3,3'-diaminobenzidine (ZLI-9019, ZSGB-BIO, China) to detect the target proteins. The intensity and density of positive cells were evaluated by ImageJ. The statistical analysis was conducted according to the method used in the TUNEL assay.

### RNA-seq

RNA-Seq was performed by Singerleron. A549-CD147-WT and A549-CD147-K71R overexpressing cells were lysed using Trizol and sent to Singerleron, and the data were analyzed, including GO analysis and KEGG pathway analysis.

### Statistical analysis

All statistical data were performed using GraphPad Prism V9.0. These experiments were performed in triplicate. Statistical analyses were performed using two-way ANOVA and unpaired *t*-test with or without Welch's correction. *P* values < 0.05 were considered statistically significant.

## Results

### The generation of anti-CD147-K71me2 antibody and identification of CD147-K71me2 in NSCLC

Protein methylation is involved in tumor progression; it has been verified that the tumor-associated antigen CD147 has various di-methylations at different lysine residues, in which the occurrence of CD147-K71me2 is relatively high.<sup>22</sup> However, the effect of this modification on NSCLC progression has not been uncovered. In order to effectively identify the level of CD147-K71me2, we generated a specific rabbit polyclonal antibody against this modification according to the procedure (Fig. 1A) and subsequently verified the specificity of the antibody. The result showed the antibody against CD147-K71me2 had a higher affinity for peptide K71me2 than peptide K71 and did not recognize peptides K148me2 and K234me2 (Fig. 1B). Meanwhile, specific peptide blocking assay showed a decreasing recognition effect on CD147-K71me2 in A549 and H460 cells and CD147-K71me2 peptide upon incubation with the mixture of CD147-K71me2 peptide and anti-CD147-K71me2 antibody, compared to anti-CD147-K71me2 antibody alone (Fig. S1A, B). The CD147 purified from A549 cells was identified by Coomassie blue staining (Fig. 1C), and detected by a pan-anti-di-methylated-lysine antibody (pan-DM) and anti-CD147-K71me2 antibody (Fig. 1D). Moreover, dot blot was used to find out the effective dilution ratio of the anti-CD147-K71me2 antibody, which showed the better distinction between peptide K71me2 and peptide K71 at 1:1600 dilution ratio (Fig. 1E). We also compared the CD147-K71me2 of His-CD147 expressed from prokaryotic expression system and H460 cells and found that CD147-K71me2 level in H460 cells was higher than that of His-CD147 (Fig. 1F). Meanwhile, CD147-WT and CD147-K71R were

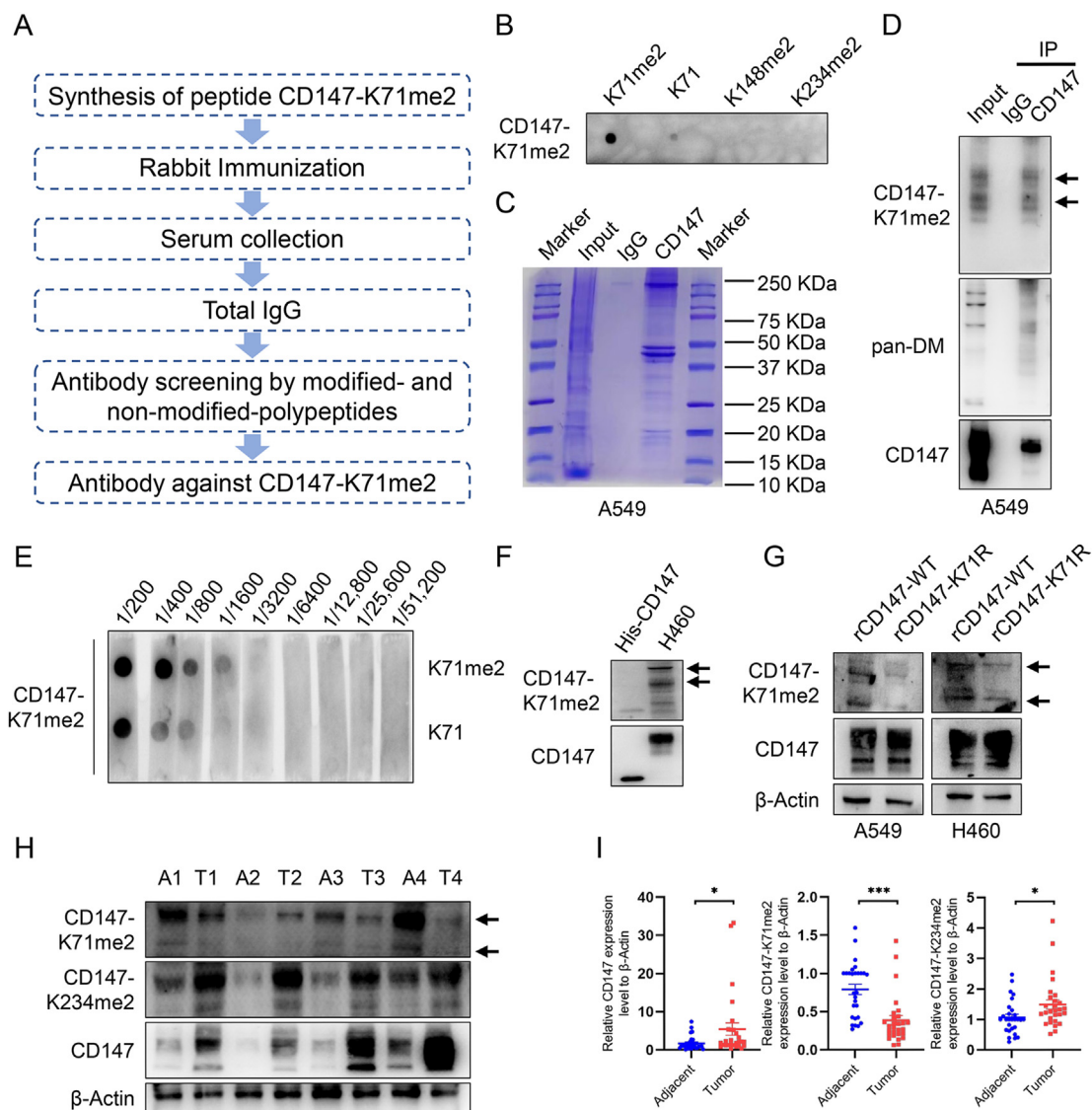


**Figure 1** The generation of anti-CD147-K71me2 antibody and identification of CD147-K71me2 in NSCLC. **(A)** The procedure of generating a specific anti-CD147-K71me2 antibody. **(B)** The specificity of the anti-CD147-K71me2 antibody was verified using dot blot. K71, K71me2, K148me2, and K234me2 were synthetic CD147 peptides. **(C)** The CD147 protein purified from A549 cells was identified by Coomassie blue staining. **(D)** The di-methylation modifications of purified CD147 were identified by Western blot using a pan-anti-di-methylated-lysine antibody (pan-DM) and anti-CD147-K71me2 antibody. **(E, F)** The specificity of the anti-CD147-K71me2 antibody was verified using dot blot (E) and Western blot (F). **(G)** The level of CD147-K71me2 in A549/H460-rCD147-WT and A549/H460-rCD147-K71R cells was detected by the anti-CD147-K71me2 antibody. **(H, I)** The level of CD147, CD147-K71me2, and CD147-K234me2 in NSCLC tissues (T;  $n = 28$ ) and adjacent tissues (A;  $n = 28$ ) was evaluated using the corresponding antibodies by Western blot (H), and statistical analysis was conducted (I). Data were presented as mean  $\pm$  SEM (\*\* $P < 0.001$ , \* $P < 0.05$ ).

overexpressed in A549/H460-shCD147 cells (Fig. S2A, B) to generate A549/H460-rCD147-WT and A549/H460-rCD147-K71R cell lines (Fig. S2C, D). The CD147-K71me2 level was detected in A549/H460-rCD147-WT and A549/H460-rCD147-K71R cells, and the result showed CD147-K71me2 level in A549/H460-rCD147-K71R cells decreased markedly compared with A549/H460-rCD147-WT cells (Fig. 1G). Subsequently, we evaluated the CD147, CD147-K71me2, and CD147-K234me2 levels of 28 NSCLC tissues and their

adjacent tissues, and observed that the CD147-K71me2 level of NSCLC tissues was lower than that of corresponding adjacent tissues, which is distinct from the high expression level of CD147 and CD147-K234me2 in tumor tissues (Fig. 1H, I; Fig. S3).<sup>22,25</sup> These findings indicate that we successfully generate a specific antibody targeting CD147-K71me2, and verify the low level of CD147-K71me2 in NSCLC tissues, indicating CD147-K71me2 may be negatively correlated with NSCLC progression.

**The methyltransferase SETDB1 catalyzes CD147 to generate CD147-K71me2**

Various methyltransferases are responsible for the generation of different protein methylations, increasing protein diversity. To screen the possible methyltransferase that catalyzes CD147-K71, we generated a siRNA library

including SETD7, SETDB1, NSD1, NSD2, SETD1A, SUV39H2, G9A, SETD6, and EZH2. Different methyltransferases were knocked down in A549 and H460 cells respectively, which has little influence on the mRNA level of CD147 (Fig. 2A–I; Fig. S4A–I). We subsequently detected the level of CD147-K71me2 in the above cells, and the result showed that CD147-K71me2 level decreased obviously in SETDB1

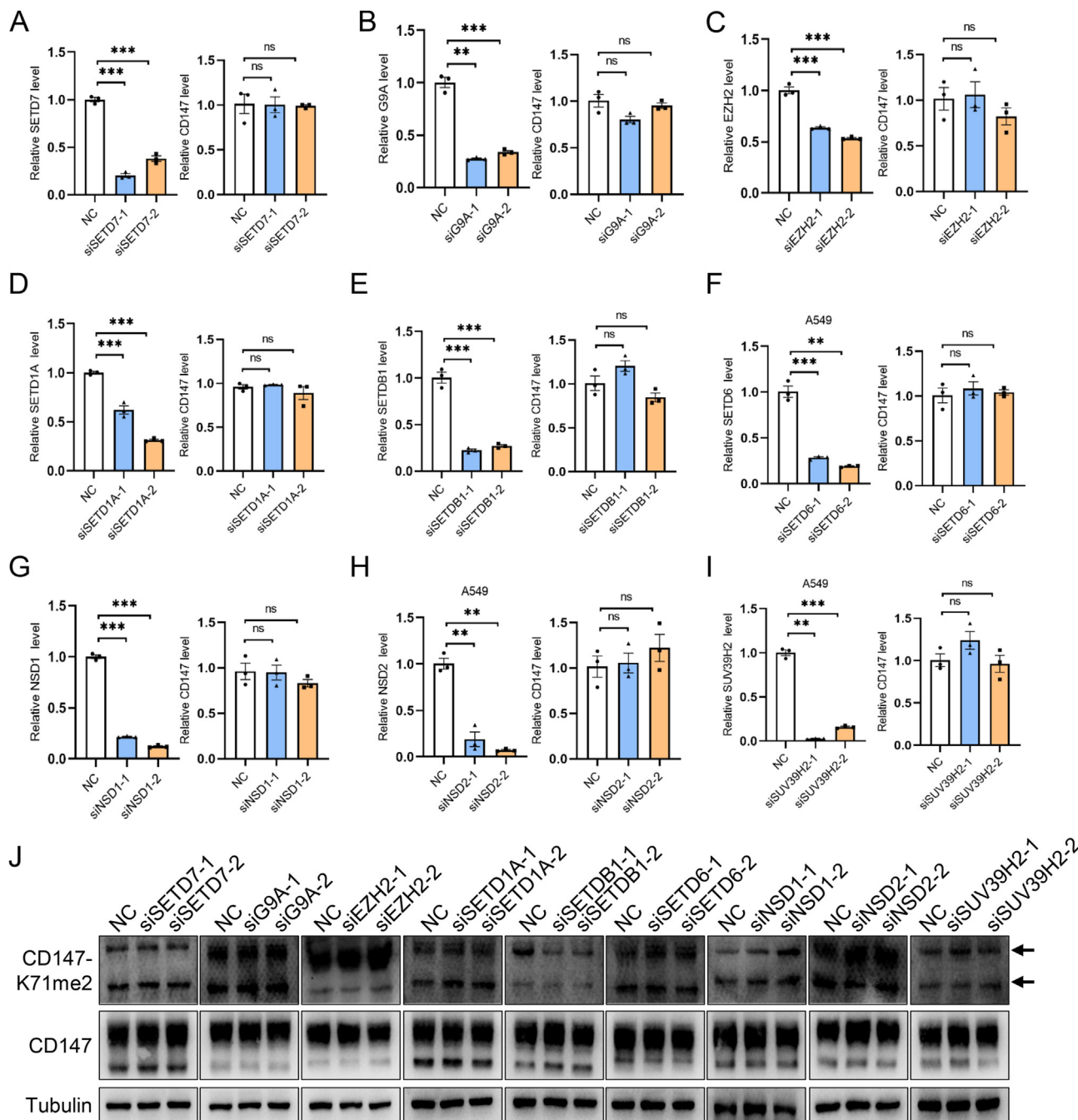


**Figure 2** SETDB1 is identified as the methyltransferase catalyzing CD147 to generate CD147-K71me2. (A–I) The mRNA levels of CD147 and different methyltransferases in A549 cells were detected after siRNA transfection by q-PCR, and statistical analysis was conducted from three independent experiments. Data were presented as mean ± SEM (\*\*\*P < 0.001, \*\*P < 0.01; ns: no significance). (J) The CD147-K71me2 level in A549 cells was evaluated after siRNA transfection by the anti-CD147-K71me2 antibody.

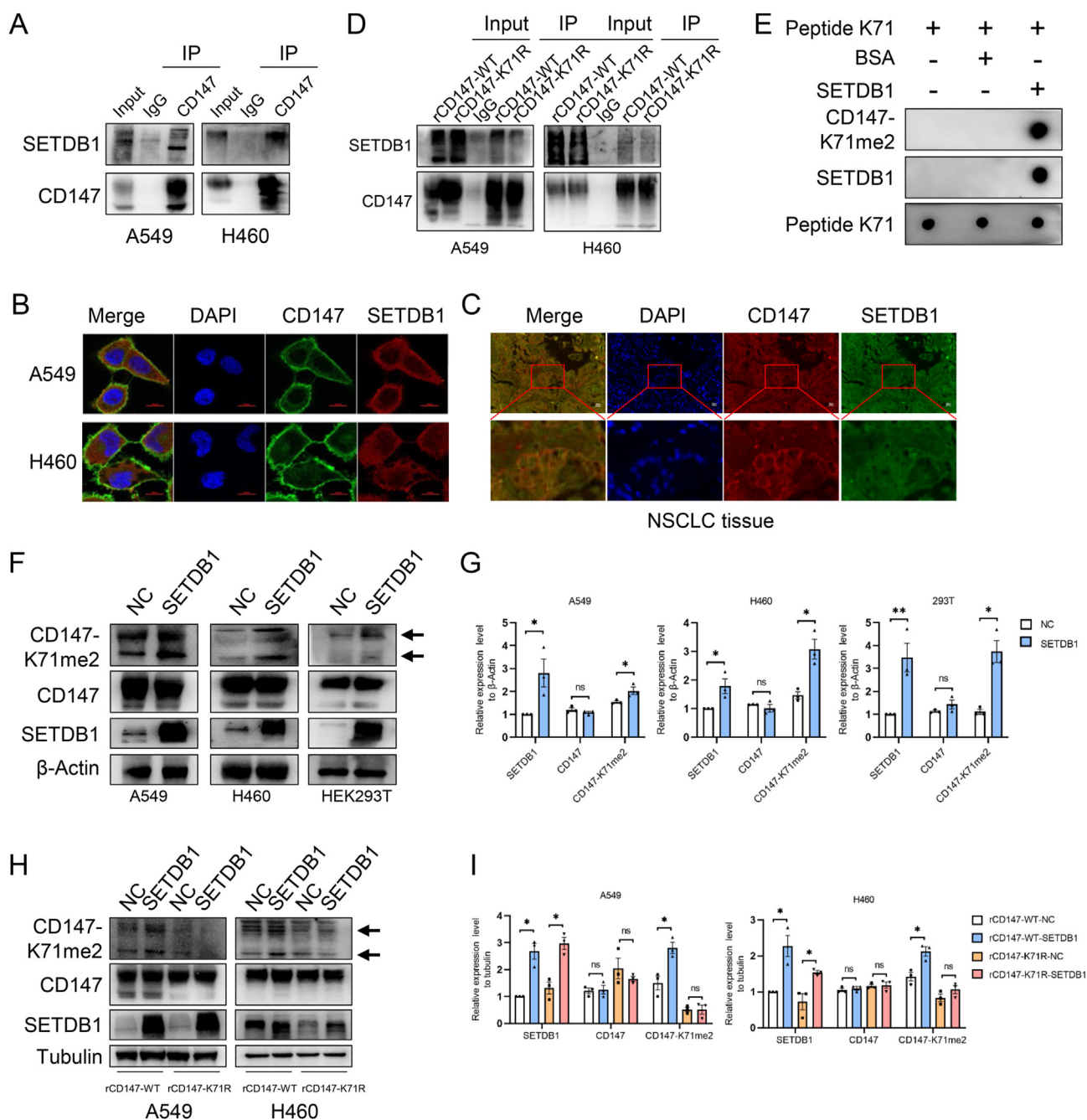


**Figure 3** SETDB1 catalyzes CD147 to generate CD147-K71me2. **(A)** The interaction between CD147 and SETDB1 was verified by Co-IP assay in A549 and H460 cell lines. **(B, C)** The co-location of CD147 and SETDB1 was evaluated by an immunofluorescence assay in NSCLC (A549 and H460) cell lines **(B)** and NSCLC tumor tissues **(C)**. Cellular immunofluorescence assay: blue, nucleus; green, CD147; red, SETDB1; scale bar = 10  $\mu$ m. Tissue immunofluorescence assay: blue, nucleus; red, CD147; green, SETDB1; scale bar = 20  $\mu$ m. **(D)** The interaction between CD147 and SETDB1 was determined by Co-IP assay in A549-rCD147-WT/K71R and H460-rCD147-WT/K71R cells. **(E)** *In vitro* methyltransferase assay, with the peptide K71 and SETDB1 protein incubated in methyltransferase buffer. The di-methylation of peptide K71 was detected by an anti-CD147-K71me2 antibody. **(F, G)** The CD147-K71me2 level was detected in SETDB1 overexpressing A549, H460, and HEK293T cells by Western blot **(F)**, and statistical analysis was conducted using data from three independent experiments **(G)**. Data were presented as mean  $\pm$  SEM (\*\* $P$  < 0.01, \* $P$  < 0.05; ns: no significance). **(H, I)** The CD147-K71me2 level was detected in SETDB1 overexpressing A549/H460-rCD147-WT and A549/H460-rCD147-K71R cells by Western blot **(H)**, and statistical analysis was conducted using data from three independent experiments **(I)**. Data were presented as mean  $\pm$  SEM (\* $P$  < 0.05; ns: no significance).

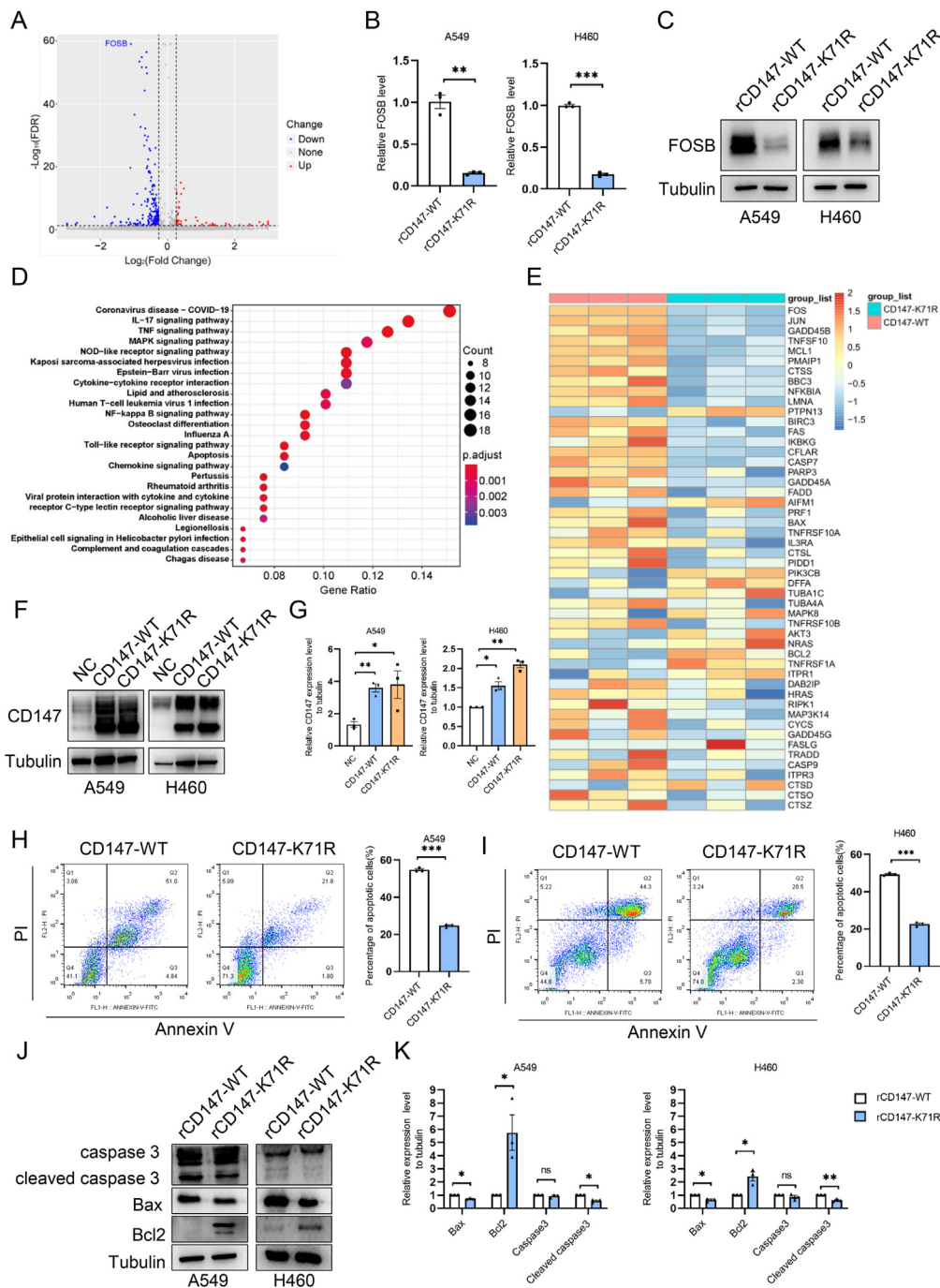


**Figure 4** CD147-K71me2 up-regulates FOSB expression and promotes tumor cell apoptosis. **(A)** The DEGs between A549-CD147-WT and A549-CD147-K71R cells were identified by RNA-seq analysis [fold change<sub>(CD147-K71R/CD147-WT)</sub> > 1.2 or < 0.83, FDR < 0.05]. **(B, C)** The FOSB expression levels in A549/H460-rCD147-WT and A549/H460-rCD147-K71R cells were detected by q-PCR **(B)** and Western blot **(C)**, respectively. **(D)** The KEGG analysis of the DEGs between A549-CD147-WT and A549-CD147-K71R cells. **(E)** The heat map showed DEGs in apoptosis pathway. **(F, G)** The CD147 expression level was detected in A549/H460-CD147-WT and A549/H460-CD147-K71R cells by Western blot **(F)**, and statistical analysis was conducted using data from three independent experiments **(G)**. Data were presented as mean  $\pm$  SEM (\*\* $P$  < 0.01, \* $P$  < 0.05). **(H)** The percentage of apoptotic cells was detected in A549-CD147-WT and A549-CD147-K71R cells after the stimulation of cisplatin (4  $\mu$ g/mL) by flow cytometry and statistical analysis was conducted using data from three independent experiments. Data were presented as mean  $\pm$  SEM (\*\*\* $P$  < 0.001). **(I)** The percentage of apoptotic cells detected in H460-CD147-WT and H460-CD147-K71R cells after the stimulation of cisplatin (4  $\mu$ g/mL) by flow cytometry and statistical analysis was conducted using data from three independent experiments. Data were presented as mean  $\pm$  SEM (\*\*\* $P$  < 0.001). **(J, K)** The expression levels of apoptotic biomarkers were detected in A549/H460-rCD147-WT and A549/H460-rCD147-K71R cells **(J)** and statistical analysis was conducted using data from three independent experiments **(K)**. Data were presented as mean  $\pm$  SEM (\*\* $P$  < 0.01, \* $P$  < 0.05; ns: no significance).

knockdown cells, while no difference was observed in other groups (Fig. 2J; Fig. S4J, 5A–I). These above results indicate that SETDB1 is a candidate methyltransferase for CD147-K71.

To further verify the above findings, the co-IP assay was performed, which showed an interaction between CD147 and SETDB1 in A549 and H460 cells (Fig. 3A). Meanwhile, the co-localization between CD147 and SETDB1 was observed in A549 and H460 cells (Fig. 3B) and NSCLC tissue (Fig. 3C). Subsequently, we performed co-IP using A549-rCD147-WT and A549-rCD147-K71R cells, and the result showed that the interaction between CD147 and SETDB1 decreased in CD147 mutant cells compared to CD147 wild-type cells (Fig. 3D). The same result was observed in H460-rCD147-WT and H460-rCD147-K71R cells (Fig. 3D). Furthermore, *in vitro* methyltransferase assay showed that SETDB1 catalyzed K71 peptide to generate the di-methylation of K71 (Fig. 3E). We also overexpressed SETDB1 in A549, H460, and HEK293T cells, and found that increased SETDB1 enhanced the level of CD147-K71me2 (Fig. 3F, G), while overexpressing SETDB1 in mutant CD147 groups had no obvious effect on CD147-K71me2 level compared to wild-type CD147 groups (Fig. 3H, I). These above results demonstrate that the methyltransferase SETDB1 catalyzes CD147 to generate CD147-K71me2.

### CD147-K71me2 up-regulates FOSB expression and promotes tumor cell apoptosis

To explore the role of CD147-K71me2 in NSCLC progression, we performed RNA-seq using A549-CD147-WT and A549-CD147-K71R cells, and genes were identified as differentially expressed genes (DEGs) if fold change<sub>(CD147-K71R/CD147-WT)</sub> > 1.2 or < 0.83 and FDR < 0.05. The results showed that 59 up-regulated genes and 218 down-regulated genes were identified in the mutant CD147 group compared to the wild-type CD147 group (Fig. 4A). Among these DEGs, FOSB was identified as the most significant DEG, and validated by q-PCR and Western blot (Fig. 4B, C). Furthermore, we conducted a KEGG analysis on the DEGs, and the result showed that the DEGs were closely related to several tumor-associated pathways, including “IL-17 signaling pathway”, “TNF signaling pathway”, “MAPK signaling pathway”, “NF-kappa B signaling pathway”, and “Apoptosis” (Fig. 4D). FOSB has been identified as a subunit of activator protein 1 (AP-1), which participated in cell proliferation and apoptosis.<sup>26</sup> Subsequently, we evaluated cell proliferation between the wild-type CD147 group and the mutant CD147 group, and the results showed that no statistical difference was shown between both groups (Fig. S6A, B). Thus, we analyzed the DEGs enriched in apoptosis and found that the expression level of pro-apoptotic protein Bax in the CD147-K71R group was lower compared with the CD147-WT group, while the expression level of anti-apoptotic protein Bcl2 showed the opposite trend (Fig. 4E). These findings suggest that CD147 up-regulates the FOSB expression level and may contribute to cell apoptosis. To validate the role of CD147-K71me2 in cell apoptosis, we constructed plasmid pcDNA3.1-CD147-K71R based on the plasmid pcDNA3.1-CD147-WT and the two plasmids were transfected into A549 and H460 cells (Fig. 4F, G). Then, flow cytometry was performed to

evaluate the percentage of apoptotic cells after 48-h stimulation of cisplatin. The results showed that the percentage of apoptotic cells in the mutant group decreased significantly compared with the wild-type CD147 group (Fig. 4H, I). Meanwhile, we detected the expression level of Bcl2, Bax, and cleaved caspase 3, and observed that the expression level of Bax and cleaved caspase 3 in the mutant group decreased compared to the wild-type group, while the expression level of Bcl2 showed an increasing trend in the mutant group (Fig. 4J, K). These above results indicate that CD147-K71me2 promotes NSCLC cell apoptosis.

### CD147-K71me2 promotes cell apoptosis through p38 signaling pathway

MAPK signaling pathways play a crucial role in cell apoptosis through AP-1.<sup>26,27</sup> Thus, we detected the activation of MAPK signaling pathways and observed that only the phosphorylation of p38 was down-regulated in the CD147 mutant cells, while the phosphorylation of ERK1/2 and JNK did not change compared to CD147 wild-type cells (Fig. 5A, B). Subsequently, we detected the percentage of apoptotic cells in the wild-type and mutant groups after adding p38 inhibitor (SB203580) under the stimulation of cisplatin, and observed a more significant decrease in the percentage of apoptotic cells in the wild-type group after adding p38 inhibitor compared to the mutant group (Fig. 5C–F), indicating that CD147-K71me2 promoted cell apoptosis through p38 signaling pathway. Furthermore, we detected the expression level of FOSB after adding p38 inhibitor in A549 cells, and the results showed that FOSB expression decreased in the wild-type group, while no change was found in the mutant group (Fig. 6A). To explore the role of FOSB, we knocked down FOSB in A549 cells, and the results showed that FOSB was knock-downed successfully using corresponding siRNAs (Fig. 6B). Then, we detected the percentage of apoptotic cells in the wild-type and mutant groups after transfection with FOSB siRNA-1 and siRNA-2 under the stimulation of cisplatin, and a more significant decrease in the percentage of apoptotic cells in wild-type group compared to the mutant group (Fig. 6C, D). Meanwhile, we detected the expression level of Bcl2 by Western blot after siRNA transfection targeting FOSB in A549 cells, and found that the Bcl2 level increased upon siRNA transfection (Fig. 6E). These above results indicate that CD147-K71me2 up-regulates the expression level of FOSB through p38 signaling pathway, contributing to cell apoptosis.

### CD147-K71me2 inhibits NSCLC progression by promoting cell apoptosis

To further validate the role of CD147-K71me2 in NSCLC progression, *in vivo* experiment was conducted by injecting A549-rCD147-WT and A549-rCD147-K71R cells into nude mice (Fig. 7A). Then, we measured the volume and weight of the tumors, and found that the volume in mutant CD147 group was bigger than that in wild-type CD147 group (Fig. 7B). We also observed a heavier weight in mutant CD147 group compared to wild-type CD147 group (Fig. 7C). Subsequently, we detected the level of CD147-K71me2, FOSB, Bcl2, Bax, and p38, and the phosphorylation level of

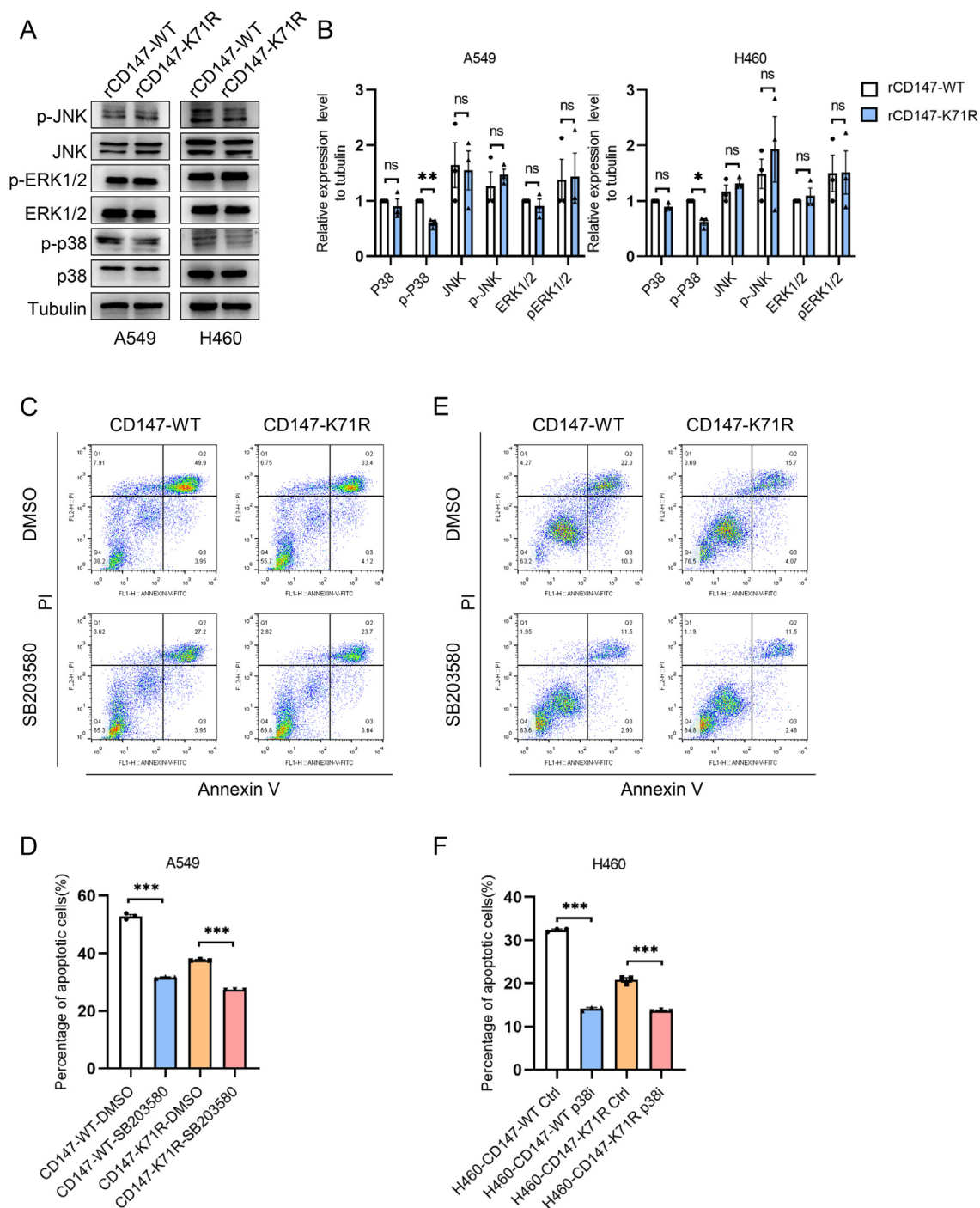


**Figure 5** CD147-K71me2 promotes cell apoptosis through p38 signaling pathway. **(A, B)** The activation of three typical MAPK signaling pathways was detected in A549/H460-rCD147-WT and A549/H460-rCD147-K71R cells **(A)** and statistical analysis was conducted using data from three independent experiments **(B)**. Data were presented as mean  $\pm$  SEM ( $^{**}P < 0.01$ ,  $^{*}P < 0.05$ ; ns: no significance). **(C, D)** The percentage of apoptotic cells in A549-CD147-WT and A549-CD147-K71R cells was evaluated after adding p38 inhibitor (SB203580) under the stimulation of cisplatin **(C)** and statistical analysis was conducted using data from three independent experiments **(D)**. Data were presented as mean  $\pm$  SEM ( $^{***}P < 0.001$ ). An equal amount of DMSO was added as a control. **(E, F)** The percentage of apoptotic cells in H460-CD147-WT and H460-CD147-K71R cells was evaluated after adding a p38 inhibitor (SB203580) under the stimulation of cisplatin **(E)** and statistical analysis was conducted using data from three independent experiments **(F)**. Data were presented as mean  $\pm$  SEM ( $^{***}P < 0.001$ ). An equal amount of DMSO was added as a control.

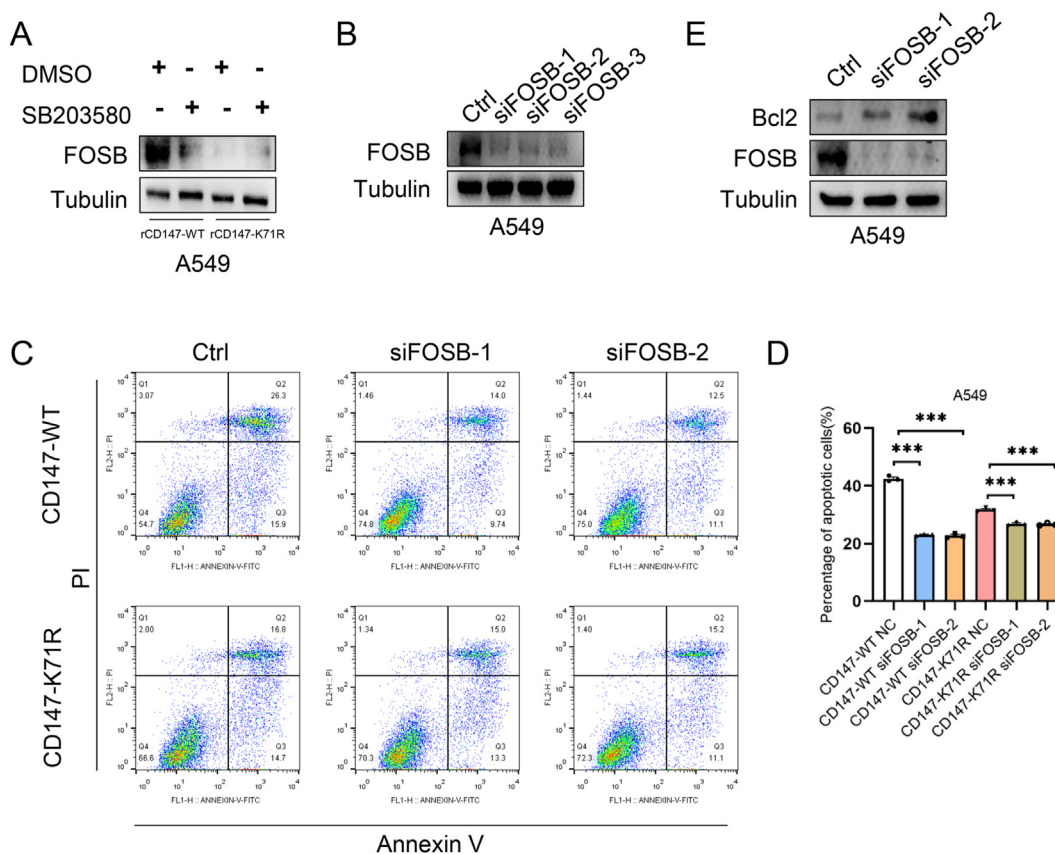


**Figure 6** CD147-K71me2 promotes cell apoptosis through the regulation of FOSB. (A) FOSB expression level in A549-rCD147-WT and A549-rCD147-K71R cells was detected after adding a p38 inhibitor (SB203580). An equal amount of DMSO was added as a control. (B) FOSB expression level was detected after FOSB siRNA transfection in A549 cells by Western blot. (C, D) The percentage of apoptotic cells in A549-CD147-WT and A549-CD147-K71R cells was evaluated after FOSB siRNA transfection under the stimulation of cisplatin (C) and statistical analysis was conducted using data from three independent experiments (D). Data were presented as mean  $\pm$  SEM ( $***P < 0.001$ ). (E) Bcl2 expression level was detected in A549 cells after siRNA transfection targeting FOSB by Western blot.

p38 in tumor tissues. We observed that the level of FOSB, p-p38, and Bax decreased with the down-regulated expression level of CD147-K71me2 in the mutant CD147 group, while Bcl2 showed an increasing trend (Fig. 7D). These results were consistent with the findings in the cellular experiments. Meanwhile, we evaluated the apoptotic level in tumors and found that the apoptotic level in the wild-type CD147 group was higher than that in the mutant CD147 group (Fig. 7E, F). Furthermore, we evaluated the expression level of Bcl2 by immunohistochemistry and found that the expression level of Bcl2 in the mutant group was higher than that in the wild-type group (Fig. 7G, H). These above results indicate that CD147-K71me2 inhibits NSCLC progression by promoting tumor cell apoptosis (Fig. 8).

## Discussion

PTMs are crucial for tumor progression,<sup>28</sup> owing to their important roles in regulating gene transcription and changing protein functions. Protein methylation is an important PTM, including histone methylation and non-histone methylation.<sup>29</sup> With the development of mass spectrometry technology, non-histone methylation attracts

increasing attention because of its profound influence on tumor progression.<sup>30,31</sup>

The tumor-associated antigen CD147 is highly expressed in a variety of tumors,<sup>32</sup> and its PTMs participate in plenty of tumor malignant behaviors. Phosphorylation is an important modification of CD147, and a low level of CD147 phosphorylation is associated with poor prognosis in hepatocellular carcinoma by promoting migration and invasion of tumor cells.<sup>33</sup> Di-methylations of CD147 at different lysine residues have already been identified in our previous work, and di-methylation of CD147-K234 contributes to NSCLC malignant behavior by enhancing glycolysis and lactate export.<sup>22</sup> Nevertheless, the role of other CD147 di-methylation in NSCLC progression remains unclear. We focus on CD147-K71me2 due to its high occurrence and find that the level of CD147-K71me2 is lower in NSCLC tissues than that in adjacent tissues, which is in contrast to its high expression in tumor tissues. RNA-seq shows that CD147-K71me2 may be associated with cell apoptosis, and we validate that CD147-K71me2 promotes cell apoptosis by detecting the percentage of apoptotic cells in CD147-WT and CD147-K71R cells, while CD147 promotes tumor progression by resisting apoptosis.<sup>20,34,35</sup> Protein methylation is crucial

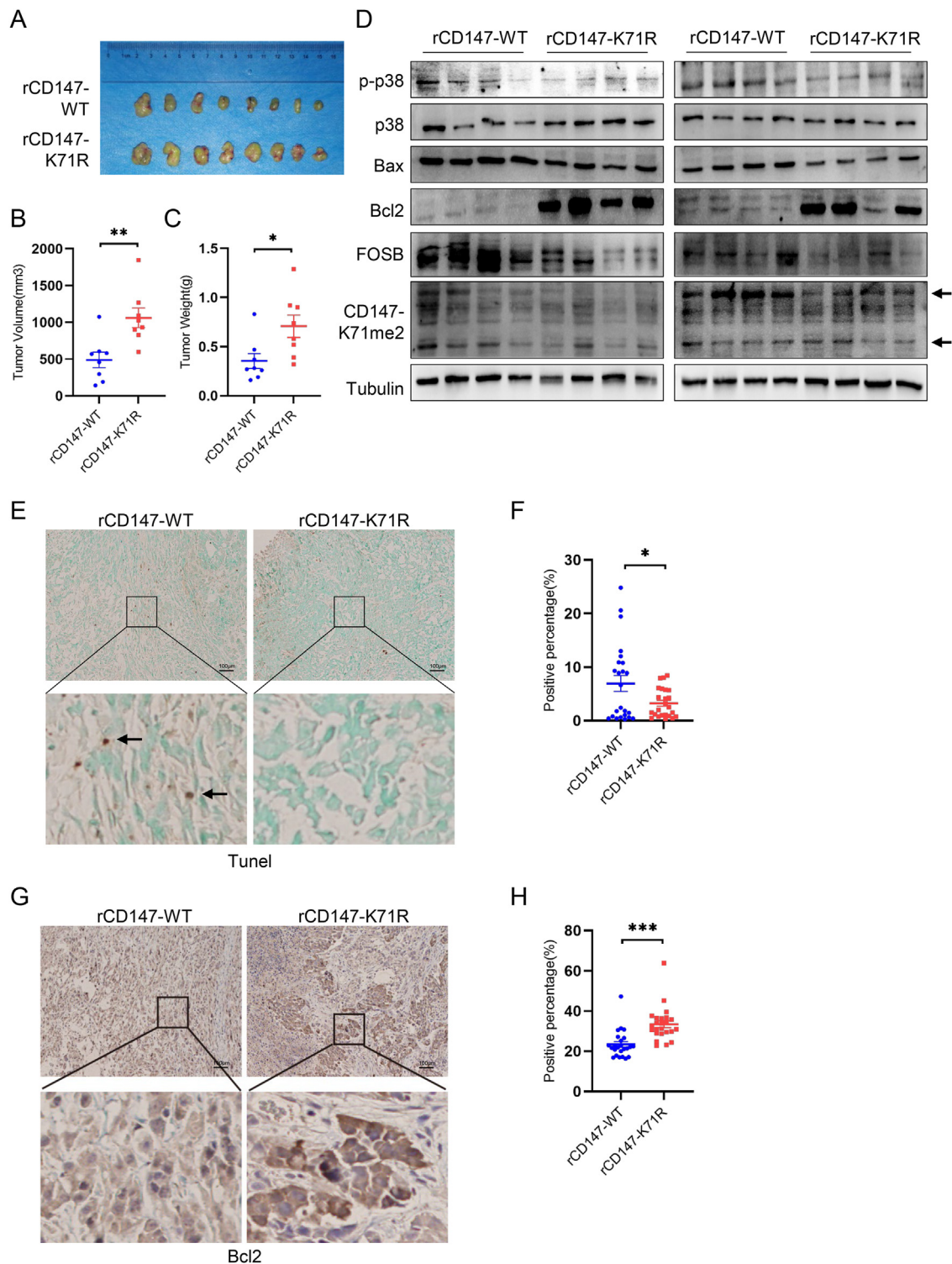


**Figure 7** CD147-K71me2 inhibits NSCLC progression by promoting cell apoptosis. **(A)** *In vivo* experiment was performed by injecting A549-rCD147-WT and A549-rCD147-K71R cells ( $2 \times 10^6$  cells) into 6-week nude mice ( $n = 8$ ). **(B, C)** Quantification of volume **(B)** and weight **(C)** of tumor masses from nude mice. Data were presented as mean  $\pm$  SEM (\*\* $P < 0.01$ , \* $P < 0.05$ ;  $n = 8$ ). **(D)** The expression levels of CD147-K71me2, FOSB, p38, p-p38, Bcl2, and Bax in tumor tissues were determined by Western blot. **(E, F)** The apoptosis of tumor tissues was evaluated by the TUNEL assay **(E)** and statistical analysis was conducted using data from three random fields of each tissue **(F)**. Data were presented as mean  $\pm$  SEM (\* $P < 0.05$ ;  $n = 24$ ; scale bar = 100  $\mu$ m). **(G, H)** The expression level of Bcl2 was determined by IHC staining **(G)** and statistical analysis was conducted using data from three random fields of each tissue **(H)**. Data were presented as mean  $\pm$  SEM (\*\* $P < 0.001$ ;  $n = 24$ ; scale bar = 100  $\mu$ m).

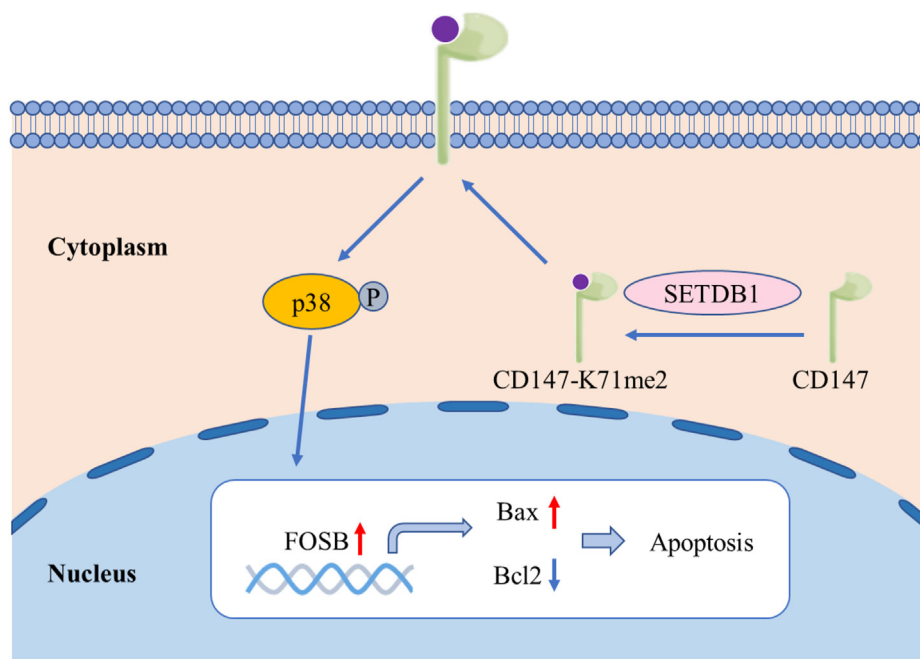


**Figure 8** Graphical abstract. Methyltransferase SETDB1-mediated CD147-K71me2 promotes FOSB expression by enhancing the phosphorylation of p38, which inhibits NSCLC progression by promoting cell apoptosis.

for increasing protein diversity, and it may play a different role from the substrate protein. P53-K370me1 catalyzed by SMYD2 represses the tumor suppressive function of p53,<sup>36</sup> and RelA-K310me1 catalyzed by SETD6 inhibits the activation of NF- $\kappa$ B-mediated inflammatory responses through attenuating RelA-driven transcriptional programs.<sup>37</sup> Hence, our findings reveal a different function of CD147 from the perspective of PTMs and may provide a reference for the research on other protein PTMs.

Protein methylation is catalyzed by different methyltransferases which are broadly divided into two groups, protein lysine methyltransferases (PKMTs) and protein arginine methyltransferases (PRMTs) according to the type of modified residues.<sup>38</sup> Methyltransferase SETDB1 is an important PKMT and catalyzes various protein methylations, which are correlated with tumor progression. The methylation of H3K9 catalyzed by SETDB1 is involved in tumor progression by silencing target gene transcription. Furthermore, the methylation of Akt catalyzed by SETDB1 promotes the oncogenic function of Akt.<sup>39,40</sup> In our study, we validated the interaction between CD147 and SETDB1 through co-IP and immunofluorescence assay and found that CD147-K71me2 level was up-regulated after over-expressing SETDB1 in A549, H460, and HEK293T cells, indicating that CD147 is a novel substrate of SETDB1.

The mitogen-activated protein kinase (MAPK) signaling pathways consist of several conventional subgroups, including ERK1/2, JNK, and p38 signaling pathways, which regulate various biological processes.<sup>41</sup> MAPKs have a dual influence on cell apoptosis through AP-1, and the cell type and stimulus determine whether they act as activators or inhibitors.<sup>27</sup> AP-1 is a mixture of dimers composed of the JUN family and the Fos family or the ATF family, and the complexity of AP-1 dimers determines the different outcomes.<sup>42</sup> FOSB, a member of the

Fos family, induces cell apoptosis in piperlongumine-treated cancer cells.<sup>43</sup> In our study, we found that FOSB expression decreased in CD147-K71R cells compared to CD147-WT cells by an RNA-seq, validated by q-PCR and Western blot. Moreover, FOSB expression was down-regulated and the percentage of apoptotic cells was also decreased after adding a p38 inhibitor. Our findings indicate that CD147-K71me2 promotes the expression of FOSB through enhancing p38 phosphorylation, leading to tumor cell apoptosis.

Our study shows that CD147 is a novel substrate of methyltransferase SETDB1, which catalyzes CD147 to generate CD147-K71me2. This di-methylation plays a different role in regulating tumor cell apoptosis compared to CD147 itself, which broadens our understanding of the role of CD147 in NSCLC progression. However, the demethylase of CD147-K71me2 has not been identified in our study, and further investigation is beneficial for us to understand the role of CD147-K71me2 in NSCLC pathogenesis.

In summary, our study demonstrates that methyltransferase SETDB1-mediated CD147-K71me2 inhibits tumor progression by facilitating tumor cell apoptosis, which enriches the role of CD147 in NSCLC progression from the perspective of PTMs.

## Ethics declaration

This study was approved by the Ethics Committee of Fourth Military Medical University.

## Author contributions

R.C., Z.N.C., and K.W. conceptualized the study, designed the experiments, and supervised the study. M.Y.S., Y.R.W., and Y.S. conducted the experiments and analyzed the data.

R.F.T. analyzed the RNA-seq data. X.H.C. and H.Z. fed the mice. M.Y.S. and K.W. wrote the original manuscript. R.C., Z.N.C., and K.W. revised the manuscript. R.C., K.W., and Y.S. performed funding acquisition and project administration. All authors read and approved the final manuscript.

## Conflict of interests

All authors have no conflict of interests.

## Funding

This work was supported by the Science and Technology Project of Shaanxi Province, China (No. 2021 PT-047, 2022 PT-43, 2022JQ-874) and the Young Elite Scientist Sponsorship Program by Cast (China Association for Science and Technology) (No. 2020QNRC001).

## Data availability

The datasets generated during and/or analyzed during the current study are available from the corresponding author upon reasonable request.

## Acknowledgements

We thank Tian-Jiao Zhang and Hai-Jiao Yang for their guidance in animal study.

## Appendix A. Supplementary data

Supplementary data to this article can be found online at <https://doi.org/10.1016/j.gendis.2023.02.015>.

## References

- Hanahan D. Hallmarks of cancer: new dimensions. *Cancer Discov.* 2022;12(1):31–46.
- Elmore S. Apoptosis: a review of programmed cell death. *Toxicol Pathol.* 2007;35(4):495–516.
- Fulda S, Meyer E, Debatin KM. Inhibition of TRAIL-induced apoptosis by Bcl-2 overexpression. *Oncogene.* 2002;21(15):2283–2294.
- Campbell KJ, Mason SM, Winder ML, et al. Breast cancer dependence on MCL-1 is due to its canonical anti-apoptotic function. *Cell Death Differ.* 2021;28(9):2589–2600.
- Wong RS. Apoptosis in cancer: from pathogenesis to treatment. *J Exp Clin Cancer Res.* 2011;30(1):87.
- Kim HS, Lee JW, Soung YH, et al. Inactivating mutations of caspase-8 gene in colorectal carcinomas. *Gastroenterology.* 2003;125(3):708–715.
- Fulda S, Küfer MU, Meyer E, et al. Sensitization for death receptor- or drug-induced apoptosis by re-expression of caspase-8 through demethylation or gene transfer. *Oncogene.* 2001;20(41):5865–5877.
- DiNardo CD, Pratz K, Pullarkat V, et al. Venetoclax combined with decitabine or azacitidine in treatment-naïve, elderly patients with acute myeloid leukemia. *Blood.* 2019;133(1):7–17.
- Roberts AW, Davids MS, Pagel JM, et al. Targeting BCL2 with venetoclax in relapsed chronic lymphocytic leukemia. *N Engl J Med.* 2016;374(4):311–322.
- Tam CS, Anderson MA, Pott C, et al. Ibrutinib plus venetoclax for the treatment of mantle-cell lymphoma. *N Engl J Med.* 2018;378(13):1211–1223.
- Macek B, Forchhammer K, Hardouin J, et al. Protein post-translational modifications in bacteria. *Nat Rev Microbiol.* 2019;17(11):651–664.
- Chandler KB, Costello CE, Rahimi N. Glycosylation in the tumor microenvironment: implications for tumor angiogenesis and metastasis. *Cells.* 2019;8(6):544.
- Chen L, Liu S, Tao Y. Regulating tumor suppressor genes: post-translational modifications. *Signal Transduct Target Ther.* 2020;5(1):90.
- Cohen HY, Lavu S, Bitterman KJ, et al. Acetylation of the C terminus of Ku70 by CBP and PCAF controls Bax-mediated apoptosis. *Mol Cell.* 2004;13(5):627–638.
- Cao J, Yan Q. Cancer epigenetics, tumor immunity, and immunotherapy. *Trends Cancer.* 2020;6(7):580–592.
- Hitosugi T, Chen J. Post-translational modifications and the Warburg effect. *Oncogene.* 2014;33(34):4279–4285.
- Kontaki H, Talianidis I. Lysine methylation regulates E2F1-induced cell death. *Mol Cell.* 2010;39(1):152–160.
- Olcina MM, Leszczynska KB, Senra JM, et al. H3K9me3 facilitates hypoxia-induced p53-dependent apoptosis through repression of APAK. *Oncogene.* 2016;35(6):793–799.
- Knutson SK, Warholc NM, Wigle TJ, et al. Durable tumor regression in genetically altered malignant rhabdoid tumors by inhibition of methyltransferase EZH2. *Proc Natl Acad Sci U S A.* 2013;110(19):7922–7927.
- Tang J, Guo YS, Zhang Y, et al. CD147 induces UPR to inhibit apoptosis and chemosensitivity by increasing the transcription of Bip in hepatocellular carcinoma. *Cell Death Differ.* 2012;19(11):1779–1790.
- Zhao S, Wu L, Kuang Y, et al. Downregulation of CD147 induces malignant melanoma cell apoptosis via the regulation of IGFBP2 expression. *Int J Oncol.* 2018;53(6):2397–2408.
- Wang K, Huang W, Chen R, et al. Di-methylation of CD147-K234 promotes the progression of NSCLC by enhancing lactate export. *Cell Metabol.* 2021;33(1):160–173.
- Li L, Tang W, Wu X, et al. HAB18G/CD147 promotes pSTAT3-mediated pancreatic cancer development via CD44s. *Clin Cancer Res.* 2013;19(24):6703–6715.
- Wu B, Zhou Y, Wang Y, et al. Dominant suppression of  $\beta$ 1 integrin by ectopic CD98-ICD inhibits hepatocellular carcinoma progression. *Int J Mol Sci.* 2016;17(11):1882.
- Li Y, Xu J, Chen L, et al. HAB18G (CD147), a cancer-associated biomarker and its role in cancer detection. *Histopathology.* 2009;54(6):677–687.
- Shaulian E, Karin M. AP-1 as a regulator of cell life and death. *Nat Cell Biol.* 2002;4(5):E131–E136.
- Yue J, López JM. Understanding MAPK signaling pathways in apoptosis. *Int J Mol Sci.* 2020;21(7):2346.
- Pan S, Chen R. Pathological implication of protein post-translational modifications in cancer. *Mol Aspect Med.* 2022;86:101097.
- Hamamoto R, Nakamura Y. Dysregulation of protein methyltransferases in human cancer: an emerging target class for anticancer therapy. *Cancer Sci.* 2016;107(4):377–384.
- Hamamoto R, Saloura V, Nakamura Y. Critical roles of non-histone protein lysine methylation in human tumorigenesis. *Nat Rev Cancer.* 2015;15(2):110–124.
- Cho HS, Shimazu T, Toyokawa G, et al. Enhanced HSP70 lysine methylation promotes proliferation of cancer cells through activation of Aurora kinase B. *Nat Commun.* 2012;3:1072.
- Riethdorf S, Reimers N, Assmann V, et al. High incidence of EMMPRIN expression in human tumors. *Int J Cancer.* 2006;119(8):1800–1810.

33. Jin J, Wang SJ, Cui J, et al. Hypo-phosphorylated CD147 promotes migration and invasion of hepatocellular carcinoma cells and predicts a poor prognosis. *Cell Oncol.* 2019;42(4): 537–554.
34. Xiong L, Edwards 3rd CK, Zhou L. The biological function and clinical utilization of CD147 in human diseases: a review of the current scientific literature. *Int J Mol Sci.* 2014;15(10): 17411–17441.
35. Ke X, Chen Y, Wang P, et al. Upregulation of CD147 protects hepatocellular carcinoma cell from apoptosis through glycolytic switch via HIF-1 and MCT-4 under hypoxia. *Hepatol Int.* 2014;8(3):405–414.
36. Huang J, Perez-Burgos L, Placek BJ, et al. Repression of p53 activity by Smyd2-mediated methylation. *Nature.* 2006; 444(7119):629–632.
37. Levy D, Kuo AJ, Chang Y, et al. Lysine methylation of the NF- $\kappa$ B subunit RelA by SETD6 couples activity of the histone methyltransferase GLP at chromatin to tonic repression of NF- $\kappa$ B signaling. *Nat Immunol.* 2011;12(1):29–36.
38. Ümit Kaniskan H, Martini ML, Jin J. Inhibitors of protein methyltransferases and demethylases. *Chem Rev.* 2018;118(3): 989–1068.
39. Wang G, Long J, Gao Y, et al. SETDB1-mediated methylation of Akt promotes its K63-linked ubiquitination and activation leading to tumorigenesis. *Nat Cell Biol.* 2019;21(2):214–225.
40. Guo J, Dai X, Laurent B, et al. AKT methylation by SETDB1 promotes AKT kinase activity and oncogenic functions. *Nat Cell Biol.* 2019;21(2):226–237.
41. Kholodenko BN, Birtwistle MR. Four-dimensional dynamics of MAPK information-processing systems. *Wiley Interdiscip Rev Syst Biol Med.* 2009;1(1):28–44.
42. Ameyar M, Wisniewska M, Weitzman JB. A role for AP-1 in apoptosis: the case for and against. *Biochimie.* 2003;85(8): 747–752.
43. Park JA, Na HH, Jin HO, et al. Increased expression of FosB through reactive oxygen species accumulation functions as pro-apoptotic protein in piperlongumine treated MCF<sub>7</sub> breast cancer cells. *Mol Cell.* 2019;42(12):884–892.